DYNAMIC CHARACTERISTICS OF A MILLIMETER-SIZED MAGNETIC BEARING WITH A CYLINDRICAL ROTOR

Mochimitsu Komori,[1] Hirotsugu Kobayashi,[1] Masahiro Kumamoto[1]

ABSTRACT

In order to study contact-free levitation systems for micromachines, our group has developed a bearing system with a millimeter-sized cylindrical rotor. The system consists of a rotor (2.0mm ϕ $\times$8mm, 95mg), a pair of electromagnets for levitation, two pairs of photo diodes for sensing, and an analog PD controller. The photo diodes detect axial displacements and rotation speeds of the rotor. This paper describes the dynamic characteristics of the millimeter-sized rotor. From the results, it is found that the levitating rotor makes a very quick response and the magnetic friction is dominant for the rotation decays. Furthermore, our group has succeeded in applying the small cylindrical rotor to the PM type motor.

INTRODUCTION

Various kinds of micromachines fabricated by IC process techniques have been proposed (Mehregany et al.,1989; Guckel et al. 1991). According to these papers, mechanical frictions and pneumatic viscosities in micromachines are more dominant compared with normal-size machines for their practical use. Furthermore, several levitation-type micromachines have been proposed (Kim, et al., 1989; Pister, et al., 1990; Siegwart, et al., 1994; Bleuler, et al., 1994; Mueller, et al., 1996; Komori, et al., 1996). Among them, there are a few reports on small-sized active magnetic bearings (AMB) (Siegwart, et al., 1994; Bleuler, et al. 1994; Mueller,et al. 1996; Komori, et al. 1996). However, there are not so many reports on small magnetic bearings with cylindrical rotors.

Our group has developed a magnetic bearing system with a cylindrical rotor (Komori, et al. 1996). Since our system has a very small rotor, the system is considered to have dynamic characteristics different from normal-sized AMB systems. This paper discusses the dynamics of the magnetic bearing system with a millimeter-sized cylindrical rotor and a PM type motor as an application with the bearing system.

Kyushu Institute of Technology, Kawazu, Iizuka, Fukuoka 820-8502, Japan.

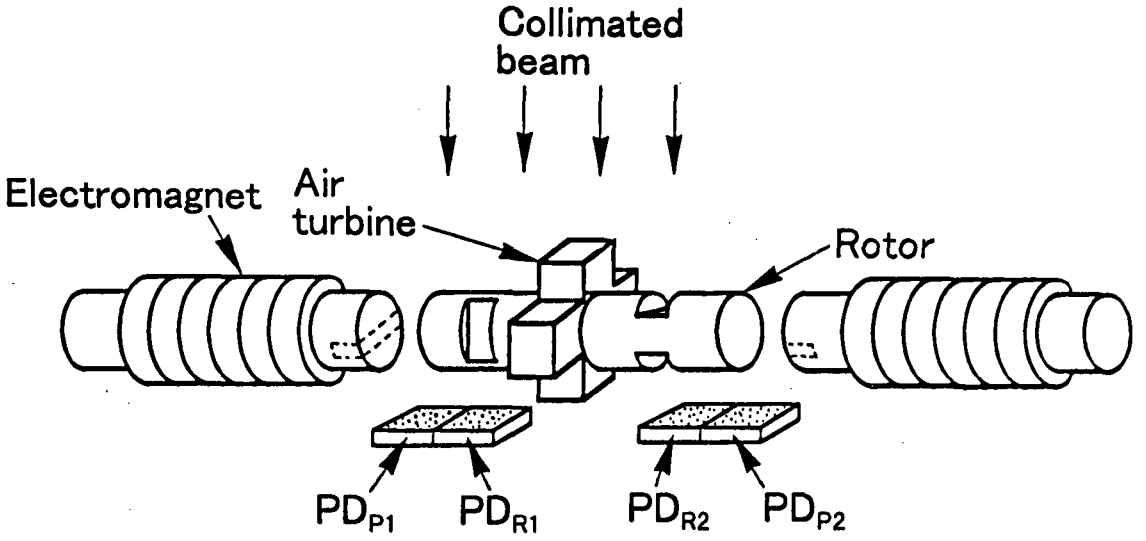

Figure 1. Illustration of a magnetic bearing system with a millimeter-sized rotor. The system consists of a rotor, a pair of electromagnets, two pairs of photo diodes, and a PD controller.

SYSTEM

Figure 1 shows an illustration of the millimeter-sized magnetic bearing system. As shown in Fig.1, the system consists of a cylindrical rotor, a pair of electromagnets, two pairs of photo diodes. The rotor is made of iron, and measures 2.0mmϕ in diameter, 8.0mm in length, and 95mg in weight. Two pairs of depressions ($\approx 1.0 \times 1.0 mm^2$) are in the rotor to detect the rotation angle as shown in Fig.1. The rotor is supported by the electromagnets just in the axial direction. In this system, the radial displacement is passively stabilized by the electromagnets. The electromagnets' cores are cylindrical irons of 2.0mmϕ $\times$20mm. Photo diodes PD_{P1}, PD_{P2} , PD_{R1}, PD_{R2} are placed under the rotor. Collimated beam throws the rotor shadow over the photo diodes. Thus, the photo diodes can detect the rotor position. Four air turbine blades ($1.0 \times 1.0 \times 1.0 mm^3$) are attached to the rotor. Compressed air turns the rotor at a desired speed. The gaps between the rotor and the electromagnets are so small that it's difficult to measure the density in the gaps. Here, we measure the magnetic force between the rotor and the electromagnets instead of measuring the magnetic flux density. The details of system specifications are shown in Table 1.

Figure 2 shows an illustration for sensing principal in the axial displacements and the rotation speeds. The illustration is a top view of the magnetic bearing system. V_1 is a differential output voltage from the photo diodes PD_{P1}, PD_{P2} , and V_2 is a differential output voltage from the photo diodes PD_{R1} and PD_{R2} . The sensing in the experiments is performed by the differential measurement principle. The photo diodes PD_{P1}, PD_{P2} can

Table 1. System specifications containing PD gains used in the bearing system.

Parameter	Value	Unit
Magnetic Face Area	3.14×10^{-6}	m^2
Turns of Magnet Wire	160	
Wire Diameter of Magnet Coil	0.3	mm
Bias Current in for Electromagnets	0.4	A
Power Amplifier Gain k_a	0.2	A/V
Current stiffness	0.130	N/A
Position stiffness k_m	456	N/m
Air Gap Length	0.1×10^{-3}	m
Rotor Mass m	95×10^{-6}	kg
Rotor Length	8.0×10^{-3}	m
Rotor Diameter	2.0×10^{-3}	m
Moment of Inertia J	4.75×10^{-11}	kgm^2
Displacement Sensor Gain k_s	2.0×10^{4}	V/m
Proportional gain K_P	13.6	
Derivative gain K_D	2.36×10^{-3}	
Time constant K_{Ds}	1.0×10^{-5}	s^{-1}

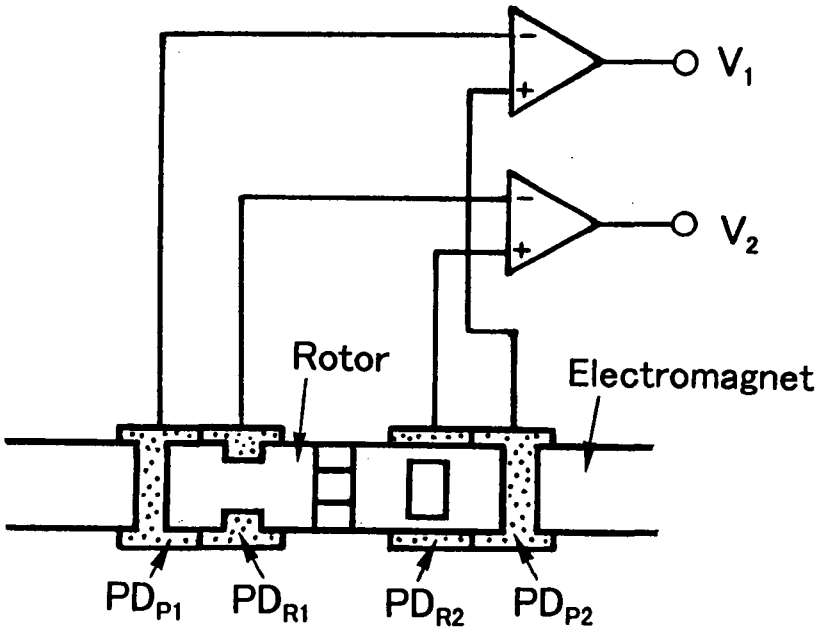

Figure 2. Sensing of the axial displacements and the rotation speeds. The schematic illustration is a top view of the bearing system. The shadow over the photo diodes is the same as the rotor outline.

detect the axial displacements of the rotor. Therefore, the output V_1 corresponds to the rotor displacements. The sensitivity for detecting the axial displacement is 20 mV/μm as shown in Table 1. The photo diodes PD_{R1}, PD_{R2} can detect rotation angles of the rotor corresponding to the output V_2. The rotation speeds are calculated from the output period. Since the radial displacement is passively stabilized by the electromagnets, the bearing system needs only one controller in the axial direction. Thus, an analog PD controller is adopted in the rotor positioning.

ROTOR DYNAMICS

In order to study the rotor dynamics in he axial direction, the rotor motions in the frequency range less than $\approx$1.0 kHz were measured by using a digital oscilloscope. Fig.3 shows the follow-up control results of the rotor in the axial direction. The upper sinusoidal curve and the lower curve in the figure show the desired rotor displacement and the actual rotor displacement, respectively. From the result, it is found that the rotor follows up the desired displacement in the frequency range less than $\approx$1.0kHz. This result shows that the rotor can move very quickly in the axial direction. The experimental results are almost similar to the results reported elsewhere (Komori, et al. 1996).

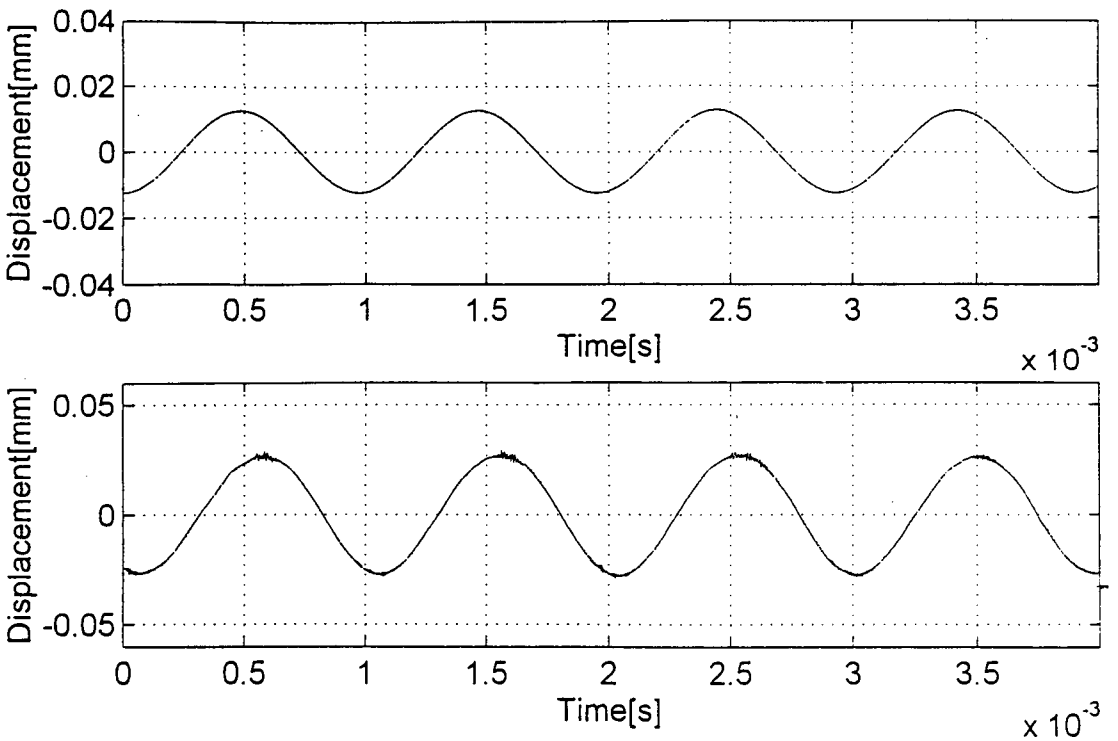

Figure 3. Follow-up control result for the levitation system. The upper sinusoidal curve and the lower one show the desired displacement and the actual displacement of the rotor, respectively.

The rotation speeds of the rotor were measured. For spinning the rotor, compressed air was applied to the rotor blades through a small nozzle (inner diameter : 0.5mmϕ). Fig.4 shows (a) the output V_2 corresponding to the rotation angles and (b) the output V_1 corresponding to the rotor displacements in the axial direction. Fig.4 (a) shows the rotation speed $\cong$ 4,000rpm, because the two periods corresponding to a rotation in the experiment are 15ms. At the rotation speed $\cong$ 4,000rpm, there is no displacement in the axial direction as shown in Fig.4(b). Fig.5 also shows (a) the output V_2 and (b) the output V_1, which correspond to the results in Figs.4(a) and (b), respectively. The result shows that the rotation speed is $\cong$ 10000rpm and that there is also no displacement in the axial direction.

Rotation speed decays were measured experimentally. In the experiment, the rotor was driven up to the desired rotation speeds by the air. Immediately after the compressed air was removed, the rotation speeds were measured. Several different initial speeds were performed. The results are shown in Fig.6. Decay curves A, B, and C in Fig.10 represent the experimental results for the initial speeds 3000, 2307, and 1395rpm. The results show that the rotor speeds decrease monotonously and the rotor for each initial speed continues to spin for a few tens seconds. In each case, the rotor continues to rotate for more than 30s.

Generally, equation for a rotation speed $\omega(t)$ without mechanical friction is represented by

$$J\,\dot{\omega}(t) + c_i\omega(t) = 0, \quad i = \text{A, B, C,} \tag{1}$$

where J is the moment of inertia for the rotor, and c_i is the coefficient of viscosity for the air. The general solution for Eq.(1) is

$$\omega(t) = \omega_0 \exp(-\frac{c_i t}{J}), \quad i = \text{A, B, C,} \tag{2}$$

where $\omega_0 = \omega(0)$. Thus, the decay curves are considered to be approximated by the exponential functions, however the curve A is fitted in the time range more than 15s. Because the rotation in the time range less then 15s is not so stable due to the passive stabilization in the radial direction. Eqs.(3)-(5) are approximation functions for the curves A, B, and C, respectively, where $\gamma_i (i = \text{A, B, C})$ are correlation coefficients.

$$\omega_A(t) = 5930\exp(-0.0759t)\ \text{[rpm]}, \quad \gamma_A = 0.996 \tag{3}$$

$$\omega_B(t) = 2370\exp(-0.0779t)\ \text{[rpm]}, \quad \gamma_B = 0.999 \tag{4}$$

$$\omega_C(t) = 1388\exp(-0.0780t)\ \text{[rpm]}, \quad \gamma_C = 0.999 \tag{5}$$

The correlation coefficients are very close to 1.0. This shows that the exponential curves of Eqs.(3)-(5) are appropriate as approximation functions.

Decay curve D with an initial rotation speed 2307rpm is a result obtained by another experimental condition. In the experiment, different electromagnets with a depression (2.0 $\times 1.0 \times 0.5\text{mm}^3$) are used in order to produce non-uniform magnetic field for the rotor. The

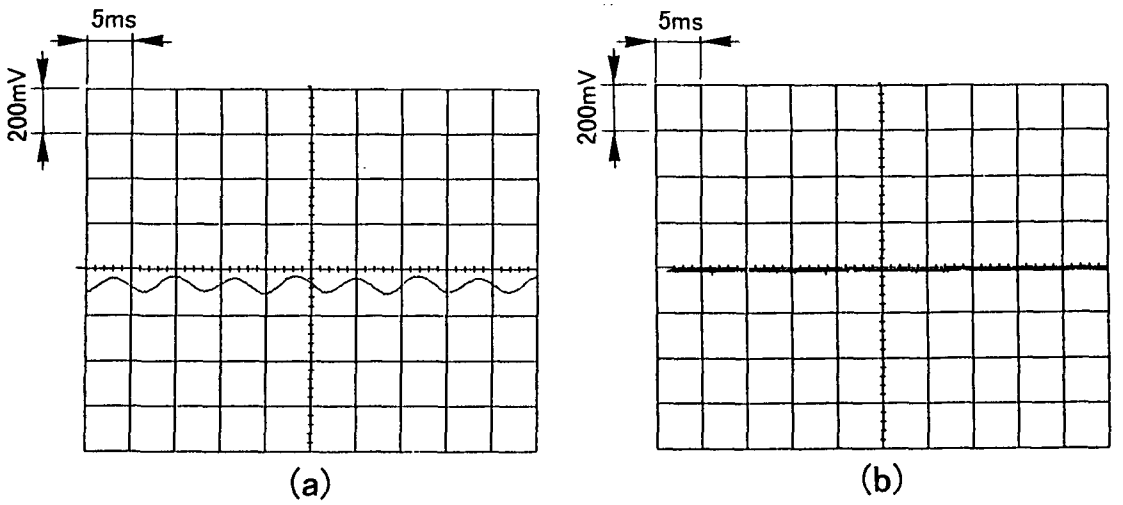

Figure 4. Experimental results for (a) the output V_2 corresponding to the rotation angles and (b) the output V_1 corresponding to the rotor displacements in the axial direction. The rotation speed shows ≅ 4000rpm.

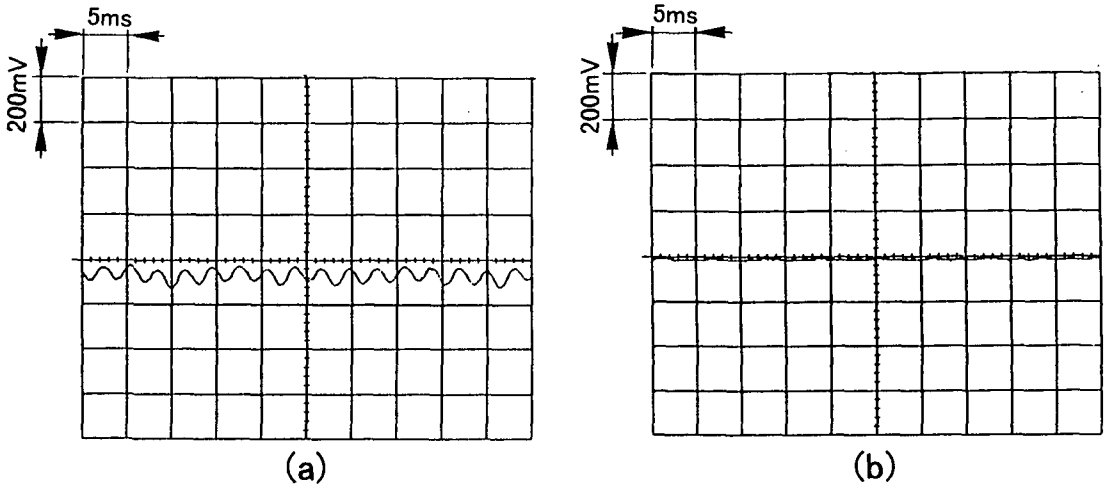

Figure 5. Experimental results for (a) the output V_2 corresponding to the rotation angles and (b) the output V_1 corresponding to the rotor displacements in the axial direction. The rotation speed shows ≅ 10000rpm.

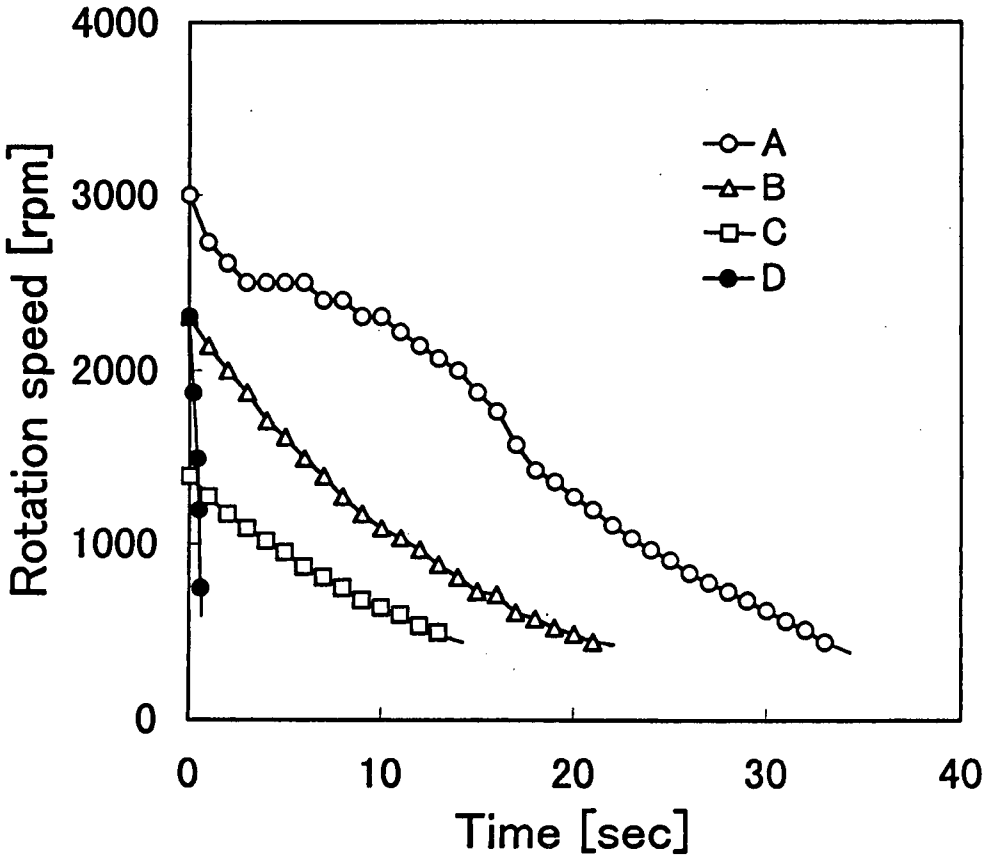

Figure 6. Rotation test results for the initial speeds of 3000, 2307, and 1395rpm, which correspond to the decay curves A, B, and C, respectively. Decay curve D with an initial rotation speed 2307rpm is a result by using electromagnets with a small depression.

depressions on the electromagnets are shown in Fig.1 as broken lines. However, other conditions for the bearing system are the same as previous conditions in the decay curves A, B, and C. The decay curve D is not applicable to an exponential function. In this case, magnetic friction due to the non-uniform magnetic field is considered to force the rotor to reduce the speed. Thus, equation for the rotation speed $\omega(t)$ with the magnetic friction is represented by

$$J\,\dot{\omega}(t) + c_D\omega(t) + r_D = 0, \tag{6}$$

Applying Maclaurin's expansion to the general solution for Eq.(6), the decay curve D is approximated by

$$\omega_D(t) = 2362 - 2457t, \quad \gamma_A = 0.972. \tag{7}$$

The linear approximation function represented by Eq.(7) is more suitable for the decay

curve D than exponential functions. From Eqs.(6) and (7), the magnetic friction $r_D = 1.1 \times 10^{-7}$[Nm] is obtained. Though the value $r_D = 1.1 \times 10^{-7}$[Nm] is very small, the magnetic friction has a large influence upon the rotation speed decay.

Our group has succeeded in applying the small cylindrical rotor to a PM type motor. Fig.7 shows the schematic illustration of (a) the PM motor and (b) the rotor with PM. The electromagnets are the same as those used in the previous experiments and a rubber ring magnet is attached to the same shaft used in the previous experiments.

With respect to the PM motor, rotation speed decays were measured experimentally. In the experiment, the rotor was driven up to the desired rotation speeds by the PM motor. Immediately after the driving currents on the PM motor were turned off, the rotation speeds were measured for several initial rotation speeds. One of the results is shown in Fig.8. Decay curves A and B are experimental results using the previous rotor with blades shown in Fig.1 and using the rotor with PM, respectively. Since the rotor shown in Fig.1 has four air turbine blades producing air friction, the air friction for the rotor shown in Fig.1 is larger than that of the rotor with PM shown in Fig.7. On the other hand, magnetic friction due to counter electromotive force is dominant for the rotor with PM motor compared with the rotor with blades. The approximation functions for the curve A and B are represented by

$$\omega_A(t) = 2688\exp(-0.0702t) \text{ [rpm]}, \quad \gamma_A = 0.998 \tag{8}$$

$$\omega_B(t) = 2679\exp(-0.151t) \text{ [rpm]}. \quad \gamma_B = 0.994 \tag{9}$$

As a result, the rotation of the rotor with PM motor decreases suddenly more than the rotor with blades in spite of existence of counter electromotive force. This shows that the magnetic friction for the rotor with PM motor is dominant in such a small magnetic bearing. The details about the dynamics on the PM motor should be studied.

SUMMARY

Our group has developed a bearing system with a millimeter-sized cylindrical rotor. The system consists of a small cylindrical rotor, a pair of electromagnets, two pairs of photo diodes, and an analog PD controller. In the experiments, It is found that for the bearing system with uniform magnetic field between the rotor and the electromagnets the rotation speed decays are represented by exponential functions and that for the bearing system with non-uniform magnetic field the rotation speed decays are represented by linear approximation functions. Furthermore, the magnetic friction for the rotor with PM is larger than that for the rotor with blades. Anyway, magnetic friction for such a small magnetic bearing system is considered to be dominant in the rotation dynamics.

REFERENCES

Bleuler,H., Kawakatsu,H., Tang,W., Hsieh,W., Miu,D.K., Tai,Y.-C., Moesner,F. and Rohner,M.

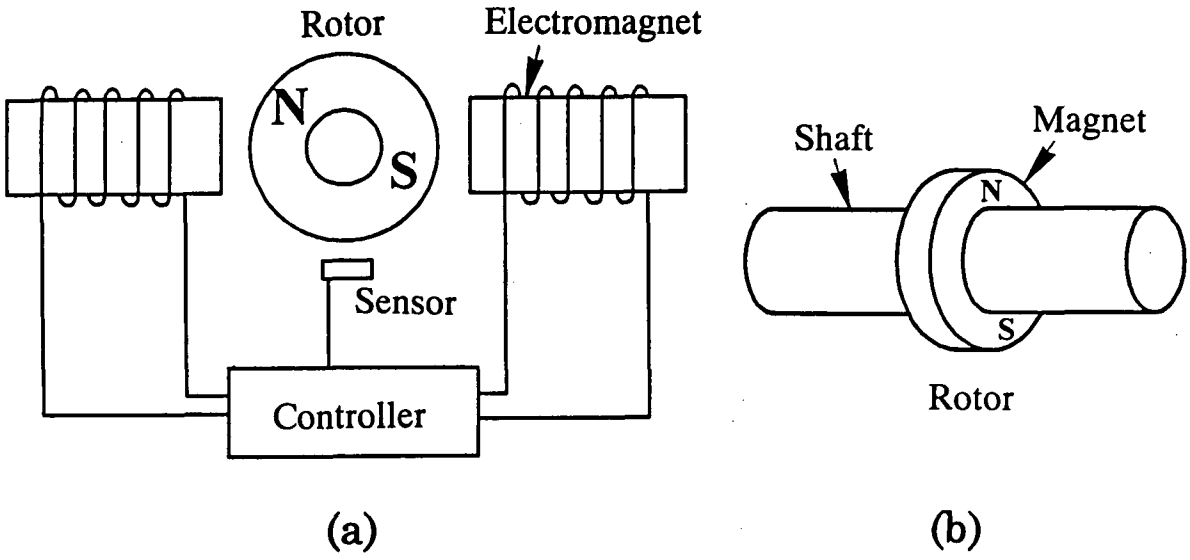

Figure 7. Schematic illustration of (a) the PM motor and (b) the PM rotor. The electromagnets are the same as those in Fig.1. A rubber ring magnet with Br=0.03Wb/m^2 is attached to the shaft used in Fig.1.

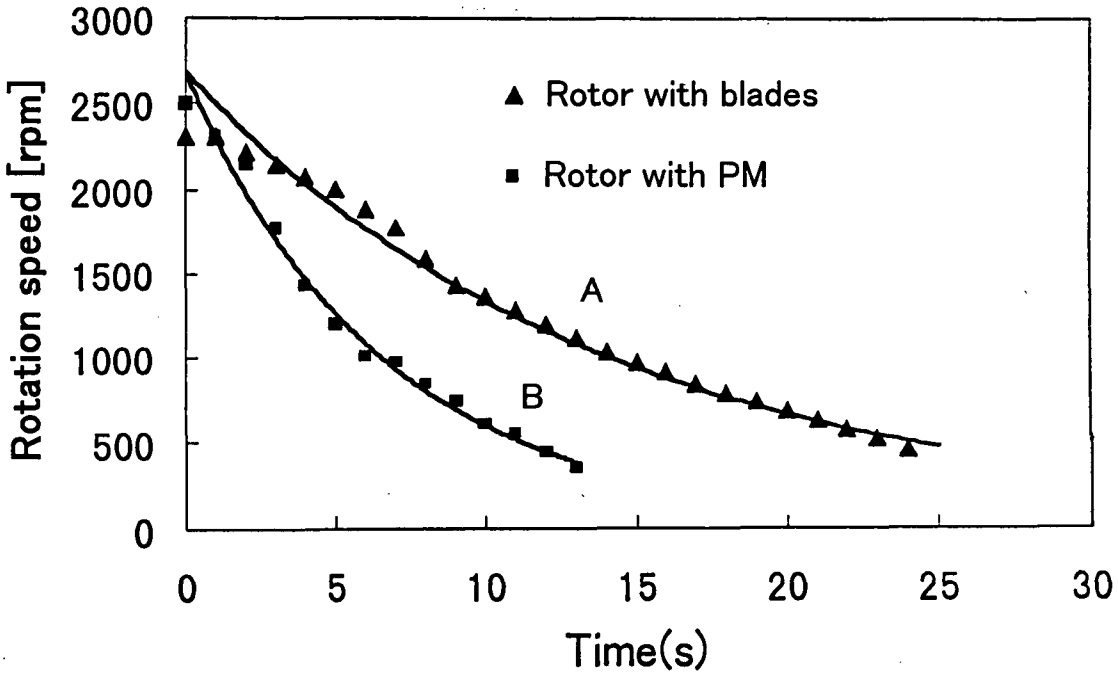

Figure 8. Rotation test results for the initial speeds of 2688 and 2679rpm, which correspond to the decay curves A and B, respectively. Decay curves A and B are experimental results using the rotor with blades and the rotor with PM.

1994. "Micromachined active magnetic bearings," *4th International Symposium on Magnetic Bearings*, Zurich, Switzerland :349-352.

Guckel,H., Skrobis,K.J., Christenson,T.R., Klein,J., Ham,S., Choi,B., Lovell,E.G. and Champman,T.W. 1991. "Fabrication and testing of the planar magnetic micromotor," *J. Micromechanics and Microengineering*, 1 (4): 135-138.

Kim,Y., Katsurai,M. and Fujita,H. 1989. "A proposal for a superconducting actuator using Meissner effect," *Proc. IEEE Micro Electro Mechanical System Workshop*, Salt Lake City, Utah, U.S.A. :107-112.

Komori,M. and Yamane,T. 1996. "Development of a millimeter-sized active magnetic bearing system," *5th International Symposium on Magnetic Bearings*, Kanazawa, Japan :405-410.

Mehregany,M., Nagarkar,P., Senturia,S.D. and Lang,J.H. 1989. "Operation of microfabricated harmonic and ordinary side-drive motors," *Proc.IEEE Micro Electro Mechanical System Workshop*, Salt Lake City, Utah, U.S.A.: 1-8.

Mueller,R., Bleuler,H., Schlaepfer,U. and Meer,M. 1996. "Active micro motor bearing," *5th International Symposium on Magnetic Bearings*, Kanazawa, Japan :401-404.

Pister,K.S.J., Fearing,R.S. and Howe,R.T. 1990. "A planar air levitated electrostatic actuator system," *Proc.IEEE Micro Electro Mechanical System Workshop*, Napa Valley, CA, U.S.A.:67-71.

Siegwart,R.Y., Bühler,P. and Baumann,D. 1994. "Eddy current bearings for micro-structure levitation," *4th International Symposium on Magnetic Bearings*, Zurich, Switzerland :359-363.